Silicon-Tungsten Calorimeter for the Forward Direction in the PHENIX Experiment at RHIC

V. Bonvicini, V. Dzhordzhadze, E. Kistenev, J. Lajoie, M. Merkine, R. Seto, and A. Vacchi

***Abstract*—The PHENIX detector at RHIC has been designed to study hadronic and leptonic signatures of the Quark Gluon Plasma in heavy ion collisions and spin dependent structure functions in polarized proton collisions. The baseline detector measures muons in two muon spectrometers located forward and backward of mid-rapidity, and measures hadrons, electrons, and photons in two central spectrometer arms, each of which covers 90° in azimuth and 0.35 units of rapidity. Further progress requires extending rapidity coverage for hadronic and electromagnetic signatures by upgrading the functionality of the PHENIX muon spectrometers to include photon and jet measurement capabilities. Tungsten calorimeters with silicon pixel readout and fine transverse and longitudinal segmentation are proposed to attain this goal. The use of such a design provides the highest density and finest granularity possible in a calorimeter.**

***Index Terms*—Analog and digital readout electronics, calorimeter, forward spectrometer, mechanical design, triggering.**

I. Introduction

THE PHENIX [1], [2] detector (Fig. 1) is designed to perform a broad study of nucleus-nucleus (A-A), proton or deuteron nucleus (p-A or d-A), and proton-proton (p-p) collisions to investigate nuclear matter under extreme conditions and spin dependent structure functions. The needs of the heavy-ion and polarized-proton programs have produced a detector with unparalleled capabilities. PHENIX measures electrons muons, photons, and hadrons with excellent energy and momentum resolution. The PHENIX detector utilizes global detectors to characterize the collisions, a pair of central spectrometers at mid rapidity to measure electrons, hadrons, and photons, and a pair of forward spectrometers to measure muons. Each spectrometer has a geometric acceptance of about one steradian and excellent particle identification.

A forward spectrometer upgrade will introduce new detector elements in the forward direction which will result in a tenfold increase in rapidity coverage for charged hadrons and photons. Forward production of inclusive jets, direct photons or Drell-Yan pairs at large x_F in nucleon-ion collisions at RHIC will provide a new window for the observation of saturation phenomena expected at high parton number densities [3], [4]. In addition these upgrades will give greater coverage for the direct photon-jet measurements, critical to the measurement of the spin dependent structure functions, and photon decays of the charmonium states such as the $\chi_C \rightarrow J/\Psi + \gamma$ for the study of charmonium suppression in heavy ion collisions.

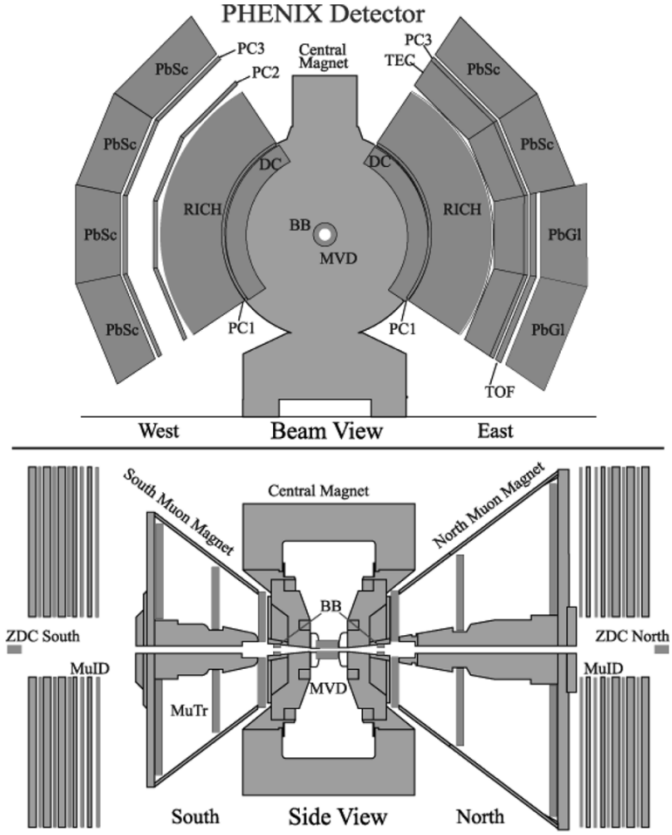

Fig. 1. A beam view (top) and side view (bottom) of the PHENIX detector in its most recent configuration. MVD—Multiplicity Vertex Detector; BB—Beam-Beam trigger counters; DC—Drift Chambers; RICH—ring imaging Cherenkov counters; PC—Pad Chambers; TEC—Time Expansion Chambers; PbSc/PbGl—Electromagnetic Calorimeters; MuTr/MuId—Muon Tracking and Muon Identification; ZDC—Zero Degree Calorimeters. There is an axial magnetic field in the central regions; the muon magnets produce a radial magnetic field.

II. PHENIX Forward Spectrometer

Currently the PHENIX Forward (Muon) spectrometers are limited to identifying muons and measuring their momenta via the muon tracker (MuTr) and the muon identifier (MuID). The three principal components to the upgrade are: 1) an enhanced

Manuscript received November 3, 2004; revised March 16, 2005. This work was sponsored by the U.S. Department of Energy under Contract no. DE-AC02-98CH1-886.

V. Bonvicini and A. Vacchi are with INFN, Sezione di Trieste, I-34127 Trieste, Italy (e-mail: bonvicini@ts.infn.it; andrea.vacchi@ts.infn.it).

V. Dzhordzhadze and R. Seto are with the University of California at Riverside, Riverside, CA 92521 USA (e-mail: seto@ucr.edu; wasiko@bnl.gov).

E. Kistenev is with the Brookhaven National Laboratory, Upton, NY 11973 USA (e-mail: kistenev@bnl.gov).

J. Lajoie is with Iowa State University and Ames Laboratory, Ames, IA 50011 USA (e-mail: lajoie@iastate.edu).

M. Merkine is with the Moscow State University, Moscow, Russia (e-mail: merkinm@silab.msu.ru).

Digital Object Identifier 10.1109/TNS.2005.852724

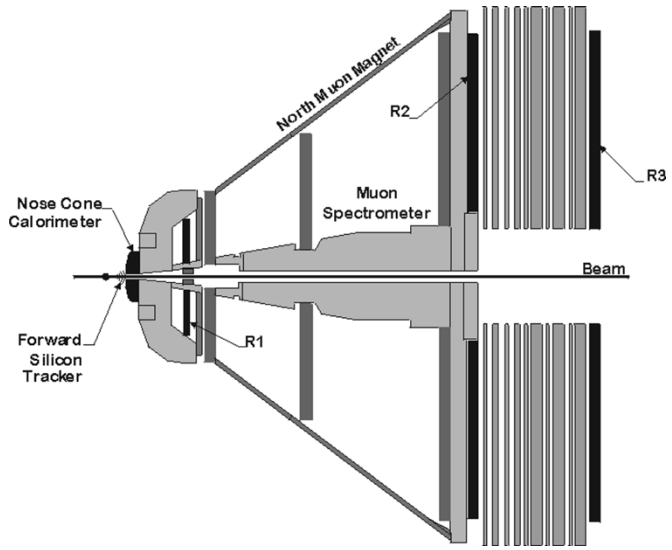

Fig. 2. Schematic rendering of the new PHENIX forward spectrometer. R1-R3—resistive plate chambers built for triggering on muons.

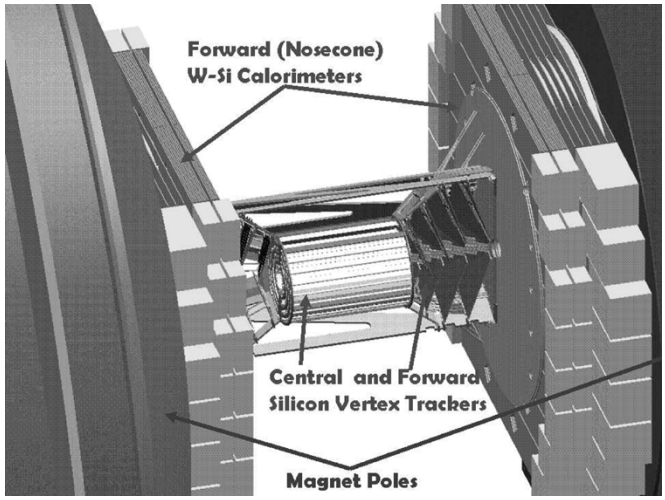

Fig. 3. Sharing of space budget between new detectors in the central PHENIX region.

muon trigger that processes signals from the R1-R3 trigger chambers which is able to recognize muons and impose cutoffs on the muon pointing and muon momenta at a RHIC rate of 10 MHz; 2) a forward Si vertex detector for identifying secondary vertices (FSVT); and 3) a compact W-Si sampling calorimeter (NCC) built to identify and measure forward electromagnetic activity and provide jet identification and coarse jet energy measurements. It is the third component which is discussed in this article. The proposed upgrade to the forward spectrometers is shown diagrammatically in Fig. 2 and further illustrated in Fig. 3.

As a component of the PHENIX Forward Spectrometer the NCC will provide or contribute to the following:

1) precision measurements of individual electromagnetic showers;
2) γ/π^0 discrimination similar to the central PHENIX electromagnetic calorimeters;
3) photon/hadron discrimination;
4) jet finding, jet energy and impact position measurements;
5) data for fast triggering.

Space for the forward upgrade is severely constrained by the existing central magnet and muon spectrometer. In particular the NCC is limited to a depth of about 20 cm, which is the depth of the present brass nose-cones, that will be replaced by this device.

III. Forward (Nose Cone) Calorimeters

A. Design and Layout

Achieving the physics goals of the experiment will require a combination of highly segmented electromagnetic and hadronic compartments supplemented by high resolution position detectors located at the depth in the calorimeter corresponding to $\sim$100% probability for *both* photons from π^0 decay to be converted and seen in the detector. The NC calorimeters are located 40 cm from the nominal collision point on both north and south poles of the PHENIX central magnet (Fig. 3). As mentioned previously, the depth of the NCC is chosen to fit within the envelope of the brass nose cones which currently occupy this space.

The unusually tight geometrical constrains of the existing PHENIX detector call for upgrade components with a very nontraditional and challenging design. The NCC is an extremely dense sampling calorimeter using tungsten absorber interleaved with silicon readout layers. The design of the NCC is based heavily on past experience in Si-W calorimetery [5]–[7] and represents a reasonable compromise between performance requirements as set by physics and the realities of PHENIX geometry. The choice of a tungsten absorber is driven by its very short radiation length and a large absorption/radiation length ratio. A few cm of tungsten will fully absorb the electromagnetic showers; hence a properly structured 20 cm deep tungsten calorimeter can have both an electromagnetic compartment and a shallow hadronic compartment. The limit to the total depth of absorber in the calorimeter is set by readout; it is our goal to reduce the readout space to about 2.5 mm per layer (0.3 mm silicon, 1.2 mm of pc-board, and 1 mm clearance gap).

To suppress the hadronic contribution to the energy seen in the electromagnetic compartment, the electromagnetic calorimeter is rather shallow—about $\sim$10 $\mathrm{L_{rad}}$ (radiation lengths) deep. The tungsten in the first 16 layers has a thickness of 2.5 mm ($\sim 0.7\,\mathrm{L_{rad}}$) and 1.6 cm in the remaining six layers. The second compartment serves the dual purposes of a hadronic energy identifier and shower tail catcher (Fig. 4).

The following characteristics will be used to identify individual hadronic and electromagnetic (EM) showers:

1) longitudinal shower profile
   a) EM showers will start in the EM compartment where most of the energy should be deposited while
   b) hadronic showers should develop later and the energy should be primarily contained in the hadronic compartment
2) lateral shower development—EM showers should be narrower than hadronic showers.

Limiting the depth of the electromagnetic compartment to $\sim$ 10 $\mathrm{L_{rad}}$ serves to improve the electromagnetic/hadronic shower

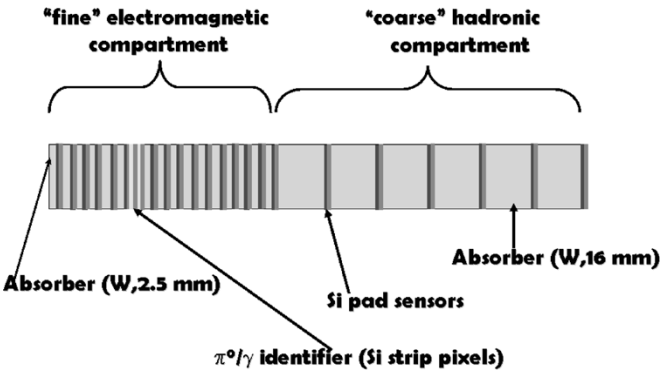

Fig. 4. Longitudinal structure of a single NCC tower.

discrimination but also results in the loss of resolution for high energy electromagnetic showers. To minimize the potential negative impact of this decision on the performance, the same lateral granularity is kept in both electromagnetic and hadronic compartments $(1.5 \times 1.5\ \mathrm{cm}^2\ \mathrm{pixels})$. Measurements in both compartments will be combined to recover the resolution.

The readout gap after layer 6 has a triple thickness to accommodate two layers of silicon strips used to discriminate between single photons and π^0's. The surface area of individual strips is chosen to be 10 times smaller than for the pixels in the remainder of the calorimeter $(\sim 15\ \mathrm{mm}^2)$ to reduce occupancy and capacitive noise. The γ/π^0 identifier will allow the identification of π^0's to 10–15 GeV/c depending on vertex position and decay configuration, and will provide additional power for electron/hadron rejection. It will also serve as an important tool for jet energy measurements, providing extra constraints on the longitudinal localization of hadronic showers, and will complement the forward tracking allowing for better matching between tracks in the FSVT and the present muon tracking system (MuTr).

The NCC has a circular geometrical coverage of a 50 cm radius corresponding to a forward rapidity range from 0.9 to 3.5 (Fig. 5). The silicon sensors will be glued to pc-boards 2 sensors wide and up to 8 sensors long $(12 \times 48\ \mathrm{cm}^2)$ thus creating readout units ready for insertion into slots between tungsten plates.

B. Front-End Electronics

The silicon tungsten calorimeter described above will have about 60 000 silicon pixels; this calls for a compact, economical readout. To control cost and complexity, we have chosen an integrated solution, where one channel of electronics serves a large number of pixels. Given a relatively modest requirement for energy resolution in the NCC's we have opted for passive summation of pixel currents from sequential detector layers either before or after the amplification.

Two different approaches to the initial stage of signal amplification are under consideration and illustrated in Fig. 6. In the case of a DC coupled detector, all input current is handled in the input amplifier (ITA—Ideal Transresistance Amplifier). In the AC case, the pixel is coupled to the amplifier through a bypass capacitor. The DC coupling scheme could be used only if the current limit set by the readout chip design (with a reasonable assumption of 100 nA per channel) is never reached.

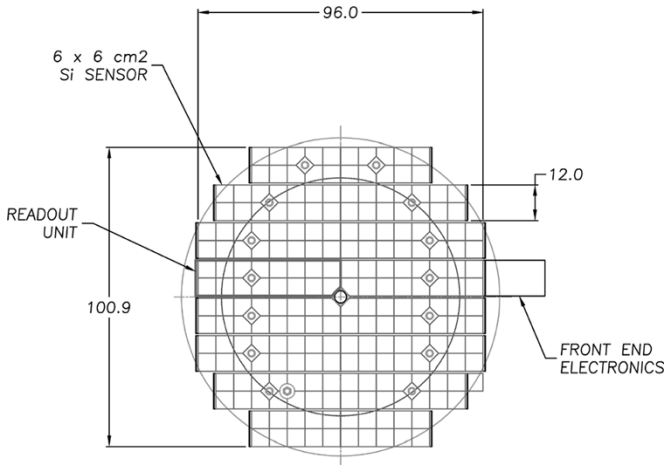

Fig. 5. NCC layout. Squares are $6 \times 6\ \mathrm{cm}^2$ Si sensors further subdivided into 16 $1.5 \times 1.5\ \mathrm{cm}^2$ pads. Signals from individual pads are carried by pc-board traces to the outer edge of the detector for summation and further processing.

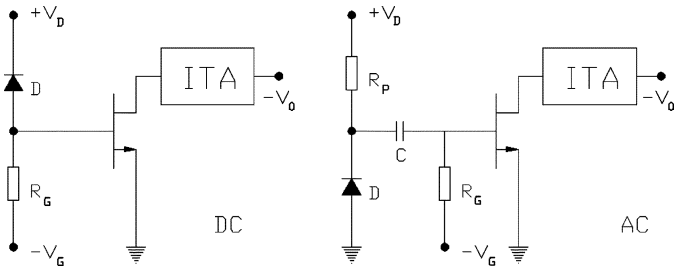

Fig. 6. Two approaches to signal processing are shown.

The preferred solution which avoids the potential of failure due to prolonged radiation exposure without large decoupling HV capacitors would be to use Si sensors with integrated capacitors. This design is unusual for pad sensors. While the technology to grow thick, large area oxide layers on silicon is not uncommon, it may result in significant cost increase due to additional technological cycles and reduced yield. All large area sensors currently used in calorimetry are DC coupled devices. Our R&D program plans for the delivery of the very first AC coupled sensors for NCC in 2005. The final choice will depend on production yield and performance of the new devices.

C. Level-1 Trigger System

The NCC will participate in a local-level-1 trigger (LL1) to select events with a high $\mathrm{p_T}$ photon or jet in the calorimeter acceptance. The processing will consist of a set of pipelined stages. First, primitive data will be built of bit-reduced digitized measurements. Second, this data will be transferred to a LL1 system, and finally, further bit-reduced trigger information will be sent to the global-level-1 trigger (GL1), via a new regional trigger processor combining level-1 information from the different forward detector systems.

The single NCC system consists of about 8 k channels of analog data per nosecone, spread over three layers in depth. The local processing units will combine calorimeter towers into nonoverlapping 2×2 trigger tiles and pass the LL1 system an 8-bit ADC value per trigger tile. The 8 bits per channel will allow a ~400 MeV least count with a full range of 100 GeV, and

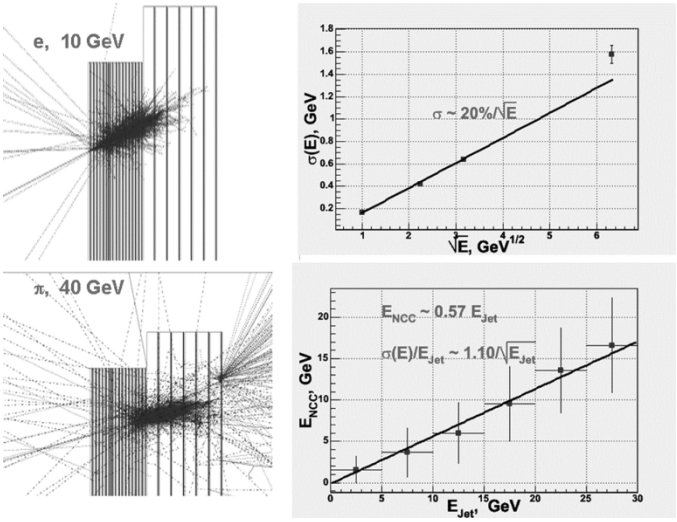

Fig. 7. NCC performance for electromagnetic shower and jet energy measurements.

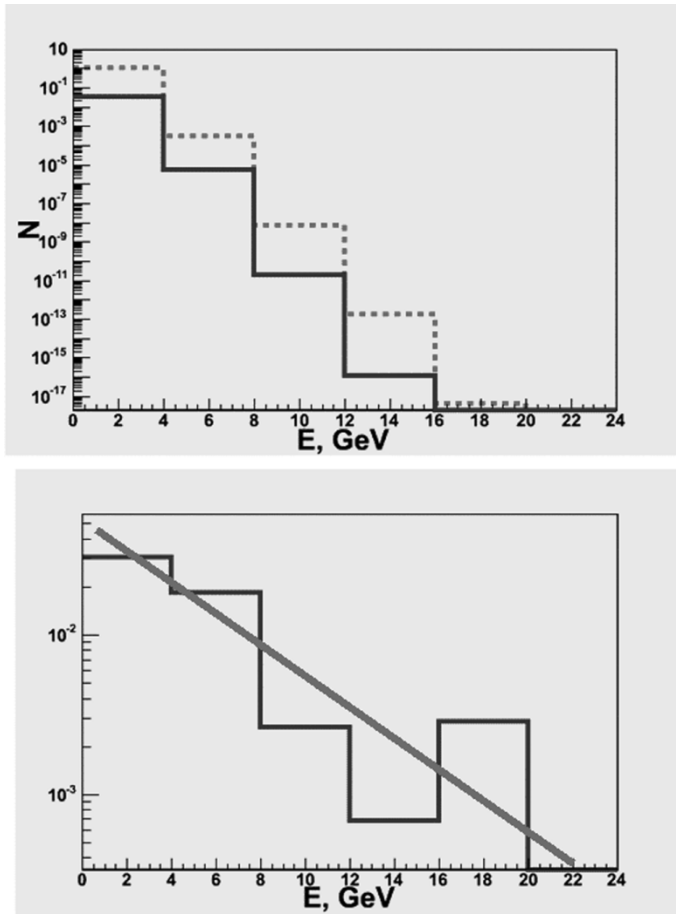

Fig. 8. Momentum spectrum of charged pions hitting the NCC in hard scattering pp events at $\sqrt{s} = 200$ GeV simulated with PYTHIA (top panel—dotted histogram) and the energy spectrum of hadronic showers passing the shower shape test applicable to electromagnetic showers (top panel—solid histogram). Testing is based solely upon *longitudinal shower shape*. The ratio of the two histograms indicating the level of suppression of charged hadrons using this method is shown in the panel at the bottom.

will result in an aggregate bandwidth of 200 Gbit/s per nosecone into the LL1 system; this is roughly a factor of 5 times larger than the data processing capacity of the existing PHENIX LL1 system.

We are considering the transfer of data over high-speed serial links into an LL1 system located in the detector hall as opposed to other LL1 systems that transmit their data over optical fiber links to LL1 electronics in the PHENIX rack room. The advantage of this approach would be that with serial links we could concentrate the entire NCC LL1 data stream into a smaller number of LL1 modules simplifying the data cross-stitching required for jet cluster trigger algorithms. This would only be possible by using high-speed copper serial links between the detector front end readout modules and the LL1 electronics which are inherently short-range—thus requiring the LL1 electronics to be located in the detector hall.

The LL1 system would provide a set of photon triggers and jet cluster triggers based on the 2×2 trigger tiles where both sets of algorithms would use information from neighboring trigger tiles and the NCC depth information to provide clean photon triggers. Detailed simulations of the performance of the NCC LL1 system are underway. The reduced bit output of the NCC LL1 trigger, in the form of a set of bits indicating satisfied algorithms, would be transmitted to the GL1 system over optical fiber.

IV. Performance

The four panels in Fig. 7 illustrate different aspects of the NCC design and performance directly related to the PHENIX experimental goals. The top right panel is the NCC photon energy resolution (in GeV) plotted as function of $\sqrt{\mathrm{E}}$. The resolution is a linear function of $\sqrt{\mathrm{E}}$ with a 20% slope up to the energies of a few tens of GeV and slightly degraded compared to this function when energy leakage to the coarse hadronic compartment becomes substantial.

Most of the electromagnetic energy stays in the electromagnetic compartments; the depth and position of those compartments with respect to shower profile are chosen to insure the linear dependence of the energy deposited in the downstream electromagnetic compartment on the momentum of the impinging photon. (A trigger on electromagnetic energy can be based upon hits in the first compartment only.) Comparable lateral and longitudinal dimensions of the individual sub towers in electromagnetic and hadronic compartments allow for independent position measurements in every compartment and provide some degree of pointing capability. Geometrically very shallow subtowers help to minimize the underlying event contribution to the measured shower energy and improve two shower separation at extreme impact angles.

Space constraints limit the total depth of calorimeter to less then $2\,\mathrm{L_{abs}}$ resulting in a substantial leakage of hadronic energy into the iron of the magnet pole backing the NCC. Comparison between energies of simulated jets and those seen in NCC (sum of energies scaled by respective sampling fractions) presented in the bottom right panel in Fig. 7 shows that jet energy measurements in this calorimeter are certainly limited by fluctuations in the amount of energy lost from leakage section. Preliminary estimates predict a jet energy resolution of about $110\%/\sqrt{\mathrm{E}}$

(Fig. 7). While jet energy measurements will have only limited validity, the fine lateral segmentation of the calorimeter will allow the measurement of the jet space vector with resolution fully satisfactory to reconstruct the kinematics of hard scattering.

It is worth noting that a tungsten calorimeter with a shallow electromagnetic compartment will have little hadronic energy deposited in that compartment. Electromagnetic showers within a jet cone identified by the energy pattern in the first two compartments will be used to improve jet energy resolution and to study modifications to jet fragmentation in nuclear matter.

A difference in the shower penetration and longitudinal shower shape serve a basis for hadron suppression and allow the NCC to be used as standalone photon identifier (Fig. 8).

The momentum spectrum of hadrons in this picture (bottom histogram) was normalized to the average hadron multiplicity in NCC. Consequently the solid histogram on the top panel can be interpreted as an expected per event multiplicity of fake electromagnetic showers. This value is to be compared to the corresponding numbers for direct photons. The latter can be estimated from PHENIX published data on π^0 and direct photon production in pp interactions at 200 GeV [8], [9]. In the pt range above 6 GeV/c where the direct photon yield exceeds 10% of the π^0 yield, i.e. ~5% of the charged hadron yield, fake electromagnetic showers are less than 1% of the total hadronic yield. This corresponds to a contamination of fake electromagnetic showers in the direct photon sample of less than 10%.

In the $\mathrm{p_T}$ range above 6 GeV/c where a direct photon yield exceeds 10% of the π^0 yield (~5% of the charged hadron yield) fake electromagnetic showers are less than 1% of the total hadronic yield corresponding to direct photon to fake electromagnetic showers ratio better than 10%.

Since the NCC is located only 40 cm from the nominal collision vertex, the job of separating single isolated photons from overlapping photons from π^0 decays is extremely challenging. The NCC design incorporates a γ/π^0 identifier built of Si strips 0.5 mm wide. Simulations show that two shower separation will be possible down to the impact point separation ~2 mm corresponding to π^0 momenta ~15 GeV. We will explore all potential algorithms for reducing the π^0 background to single photons such as independent handling of data in all three longitudinal sections to control the lateral shower shape. However, we do not expect further significant improvements to two shower separation unless the granularity is substantially increased.

ACKNOWLEDGMENT

The authors thank their PHENIX collaborators for the support and encouragement of the proposed upgrade and fruitful discussions.

REFERENCES

[1] "PHENIX Conceptual Design Report," PX20, BNL48922 internal report, 1993.

[2] M. Harrison, T. Ludlam, and S. Ozaki, Eds., "The Relativistic Heavy Ion Collider Project: RHIC and its Detectors," NIMA499, 2003. p. 235–880.

[3] R. Seto, "Future measurements at RHIC," in *Proc. Workshop on Nuclear Dynamics*, Bahamas, Jan. 2002. World Scientific 2002, nucl-ex/0204003.

[4] L. McLerran and R. Venugopalan, *Phys. Rev. D49*, p. 2233, 1994. L. McLerran, R. Venugopalan, *Phys. Rev. D49*, p. 3352, 1994. L. McLerran, R. Venugopalan, *Phys. Rev. D50*, p. 2225, 1994. See also E. Iancu, A. Leonidov, and L. McLerran, hep-ph/0202270 and hep-ph/0202025, for a nice review of the saturation and RHIC physics.

[5] I. Golutvin *et al.*, "A Silicon Hadron Calorimeter Module Operated in a Strong Magnetic Field With VLSI Read out for LHC," CERN-DRDC-91-54, CERN-DRDC-P-34, Jan 1992.

[6] J. H. Adams *et al.*, "The silicon matrix as a charge detector for the ATIC experiment," *Instrum. Exp. Tech.*, vol. 44, pp. 455–461, 2001. Prib.Tekh.Eksp. 2001 N4, 38-44, 2001.

[7] V. Bonvicini *et al.*, "New Concepts in Silicon Calorimetry for Space Experiments," NIM.A518: 186–187, 2004.

[8] S. S. Adler *et al.*, "Midrapidity neutral-pion production in proton-proton collisions at $\sqrt{\mathrm{s}} = 200\ \mathrm{GeV}$," *Phys. Rev. Lett.*, vol. 91, p. 241803, 2003.

[9] S. S. Adler *et al.*, *Mid-Rapidity Direct-Photon Production in* $\mathrm{p+p}$ *Collisions at* $\mathrm{sqrt(s)} = 200\ \mathrm{GeV}$, 2005. hep-ex/0502006.